New Journal of Physics
The open access journal at the forefront of physics

Deutsche Physikalische Gesellschaft DPG
IOP Institute of Physics

Published in partnership with: Deutsche Physikalische Gesellschaft and the Institute of Physics

OPEN ACCESS

RECEIVED
16 April 2015

REVISED
5 August 2015

ACCEPTED FOR PUBLICATION
6 August 2015

PUBLISHED
9 September 2015

PAPER

Rapid theory-guided prototyping of ductile Mg alloys: from binary to multi-component materials

Zongrui Pei[1,2], **Martin Friák**[1,2,3], **Stefanie Sandlöbes**[1,4], **Roman Nazarov**[1], **Bob Svendsen**[1,2,5], **Dierk Raabe**[1] and **Jörg Neugebauer**[1]

[1] Max-Planck-Institut für Eisenforschung GmbH, D-40237 Düsseldorf, Germany
[2] Aachen Institute for Advanced Study in Computational Engineering Science (AICES), RWTH-Aachen University, D-52062 Aachen, Germany
[3] Institute of Physics of Materials, Academy of Sciences of the Czech Republic, v.v.i., Žižkova 22, 616 62 Brno, Czech Republic
[4] Institute of Physical Metallurgy and Metal Physics, RWTH Aachen University, D-52056 Aachen, Germany
[5] Material Mechanics, Faculty of Georesources and Materials Engineering, RWTH Aachen University, D-52062 Aachen, Germany

E-mail: friak@ipm.cz

Keywords: magnesium, alloys, ductile, ternary, rare-earth, *ab initio*

Abstract

In order to identify a method allowing for a fast solute assessment without lengthy *ab initio* calculations, we analyze correlations and anti-correlation between the I_1 stacking fault energies (I_1 SFEs), which were shown to be related to the macroscopic ductility in Mg alloys, and five material parameters of 18 different elemental solutes. Our analysis reveals that the atomic volume V of pure solutes, their electronegativity ν and bulk modulus B are either linearly or logarithmically related to the I_1 SFE. Comparing the impact of solutes with that of yttrium (that increases the ductility in Mg) we propose a single numerical quantity (called yttrium similarity index, YSI) that is based on these inter-relations. Subsequently, we evaluate this new figure of merit for 76 elements from the periodic table of elements in search for solutes reducing the I_1 SFE. Limiting ourselves first to binary Mg alloys, we hardly find any alternative solutes providing similar I_1SFE reduction as that due to rare-earth (RE) additions. Therefore, we extended our search to ternary Mg alloys. Assuming that the physical properties of solute combinations can be represented by their average values, 2850 solute combinations were checked and 133 solute pairs (not including any RE elements) have been found to have a YSI larger than 0.85. Quantum-mechanical calculations have been subsequently performed for 11 solute pairs with YSIs higher than 0.95 and they were all found to reduce the I_1SFE in excellent agreement with the predictions based on the YSI.

1. Introduction

Magnesium alloys are promising structural materials due to their low weight and high specific strength [1]. However, their broader industrial applications are hindered by their low formability at ambient temperatures. The low room-temperature formability is believed to be caused by an insufficient number of active deformation modes (von Mises criterion) and is also partly associated with the highly anisotropic hexagonal close-packed (hcp) structure of Mg alloys.

It is known that the room temperature ductility of pure Mg can be significantly improved by alloying with a small amount of yttrium or other rare-earth (RE) elements [2–5]. Recent investigations have shown that the enhanced ductility in Mg-Y alloys is accompanied by an increased density of non-basal dislocations which are supposed to nucleate from I_1 stacking faults [5]. This connection between the I_1 stacking faults and non-basal dislocations has been analyzed by Agnew *et al* [6] and it has been concluded that the reaction is energetically conceivable for a wide range of fault geometries. Our previous study of this phenomenon combined quantum-mechanical (so-called *ab initio*) calculations with state-of-the-art microstructure characterization methods and resulted in a scale-bridging connection between the macroscopic ductility and atomic-scale I_1 stacking fault

energies (SFEs). We showed that the reduction of the I_1 SFE can be used as an indicator of an increased ductility in Mg alloys and, therefore, as a guiding parameter for designing new ductile Mg alloys [7].

Since RE elements are expensive due to environmental and health-risk issues related to their mining and production, it is desirable to identify alternative(s) solutes that ductilize Mg similarly as RE elements do. In our previous study [8], we selected 18 elements from the periodic table that crystallize in their pure form under ambient conditions in either hcp or double hcp (dhcp) structure. Then we performed *ab initio* calculations of the I_1 SFEs of binary Mg alloys containing these elements in solute solutions. We found that all RE elements reduce the I_1 SFE while all other non-RE elements studied increase the I_1 SFE. As RE elements are known to increase the ductility in Mg, we connect the fact that (i) RE elements reduce the I_1 SFE with (ii) the enhanced ductility in Mg alloys. Our proposed scale-bridging link was confirmed experimentally for four Mg alloys containing selected RE elements (Tb, Dy, Er and Ho).

Our approach is complementary to other scale-bridging explanations of ductility in Mg alloys. To name a few examples, Yasi and co-workers [9] simulated the core structures of basal and prismatic dislocations by the flexible boundary condition method and later developed different models to calculate the critical resolved shear stresses of basal dislocations [10] and cross-slip stresses of prismatic screw dislocations [11] in Mg alloys. As a result of these studies, low concentrations of yttrium were predicted to significantly reduce the cross-slip stress in Mg-alloys, which indicates an improved ductility of the material in agreement with our previous findings. As another example, Shin *et al* [12] applied a previously developed orbital-free density functional theory (DFT) method to dislocation core structures and subsequently calculated also Peierls stresses [13] in pure Mg. The present work extends the connection between the I_1 stacking fault and the ductility into the realm of theory-guided rapid alloy prototyping.

SFEs are among the key materials properties affecting the macroscopic mechanical behavior of metallic alloys (see, e.g., [14]). The I_1, I_2 as well as unstable stacking faults have been intensively studied in Mg [15–20]. Their simulation by quantum-mechanical methods is, however, computationally rather demanding due to the large number of atoms that need to be treated on a quantum-mechanical level. A faster approach, which does not require the use of an explicit *ab initio* SFE methodology, would be desirable for a rapid alloy design and quick selection of solutes. Therefore, in this work we systematically study correlations between SFEs in Mg alloys and properties of elemental solutes that are known and tabulated. Specifically, we analyze the relations between the I_1 SFE in Mg-*X* binaries and five different physical quantities of pure solutes: (i) their atomic volume, (ii) atomic number, (iii) I_1 SFE, (iv) electronegativity, and (v) the bulk modulus. We also analyzed the volume per atom in $Mg_{15}X$ alloys. As we find the atomic volume, electronegativity and the bulk modulus of elemental solutes clearly related to the I_1 SFE in Mg-*X* binaries, we propose a single numerical parameter containing these relations and suggest that this new figure of merit can be used as an indicator of SFE changes, and thus the ductility, in Mg alloys. The application of this new figure of merit for ternary Mg alloys is presented in the last section.

2. Computational methodology

DFT [21, 22] calculations of I_1 SFEs were carried out using the projector augmented wave (PAW) method [23] and electronic exchange-correlation effects were described by the generalized gradient approximation [24] as implemented in the Vienna Ab-initio Simulation Package (VASP) [25, 26]. A cut-off plane wave energy of 350 eV was used for all calculations of $Mg_{15}X$ alloys and elemental solutes in $2 \times 2 \times 4$ supercells. The Brillouin zones were sampled using dense Gamma-point-based $10 \times 10 \times 6$ k-point meshes to ensure the convergence of total energies within 1 meV per atom. In order to keep a similar solute concentration of both solutes in ternary Mg alloys, a 36-atom supercell $3 \times 3 \times 4$ (Mg34-*X*1-*X*2) is applied, in which there are 34 Mg atoms, one solute *X*1 and one solute *X*2. Solute *X*1 is positioned at one corner of the supercell, and solute *X*2 at its center (figure 1). The advantage of doing this is that in this case a configuration is seemingly most possible to keep the symmetry of hcp, since our yttrium similarity index (YSI) is based on hcp Mg alloys. The fact that two different solutes in supercells visualized in figure 1 are maximally separated reflects minimum interactions among different solutes that we expect in case of their dilute and low concentrations. The cut-off energy employed in computation of ternary Mg alloys is the same as in binary Mg alloys, namely 350 eV, and the gamma based k-mesh is $7 \times 7 \times 6$. These parameters guarantee total energy accuracy within 1 meV per atom. The lattice parameters of pure Mg are employed in the calculation of ternary Mg alloys, which is a good approximation as proven by testing.

Using DFT computed total energies, the I_1 SFEs were predicted in the framework of an Ising model. In this model, the total energy *E* of a sequence of hcp planes in a hcp metal is decomposed into a series where the atomic planes S_i interact via interaction energies J_i

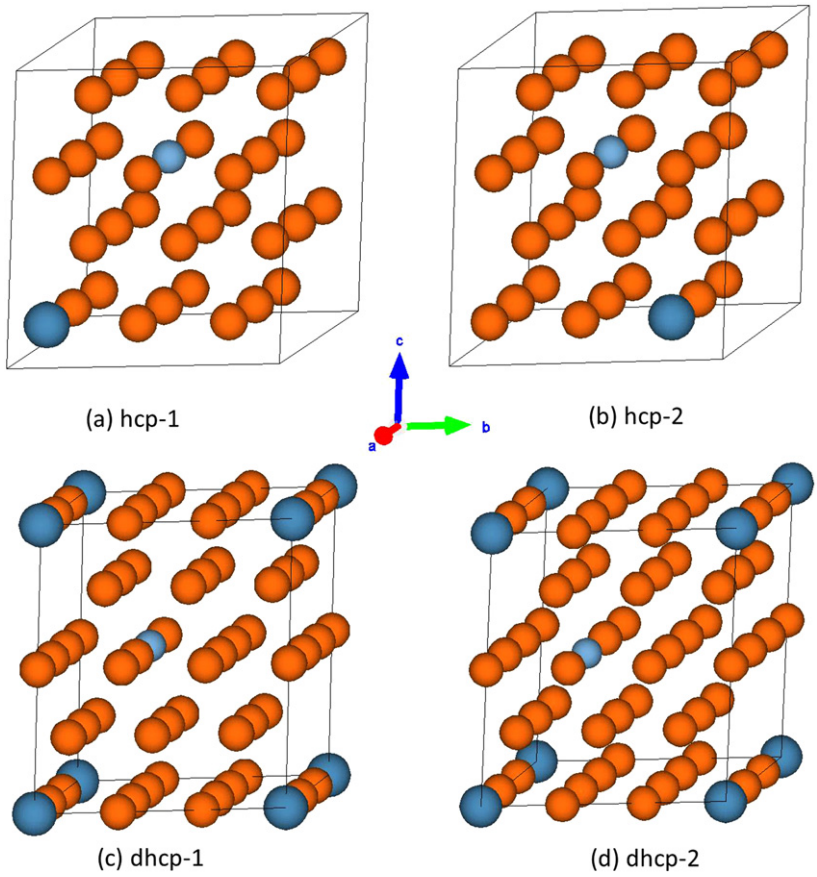

Figure 1. Schematic figure of supercells for hexagonal-close-packed (hcp) structure and double hcp (dhcp). In both hcp and dhcp there are two symmetry-nonequivalent sites for solutes *X*1 and *X*2. For convenience of description in the following text, these supercells are denoted as hcp-1, hcp-2, dhcp-1 and dhcp-2.

$$E = -\sum_{i=1}^{N}\sum_{n=1}^{N-i} J_i S_i S_{i+n}, \tag{1}$$

where n is the number of the considered neighboring planes. In the axial next nearest neighbor Ising (ANNNI) model [27, 28] only the next nearest neighbors are considered, therefore $n \leqslant 2$. The ANNNI model then results in the following expression for the I_1SF:

$$E_{I_1\mathrm{SF}} - E_0 \approx 2\left(E_{\mathrm{dhcp}} - E_{\mathrm{hcp}}\right), \tag{2}$$

where E_0 is the first term of the ANNNI model (i.e., the energy of a perfect hcp crystal). Using this expression, the SFE (defined as the energy divided by the area A of the stacking fault plane) is equal to

$$\gamma = \frac{E_{I_1\mathrm{SF}} - E_0}{A} \approx \frac{2\left(E_{\mathrm{dhcp}} - E_{\mathrm{hcp}}\right)}{A}. \tag{3}$$

This model has been successfully applied to different metals, such as fcc iron [29]. Hu *et al* [30] performed full-potential augmented plane-wave calculations using the WIEN2K code [31] for hcp Ti and hcp Re and demonstrated that the I_1 SFEs from the ANNNI model agree with those from explicit supercell calculations. We note that the use of the ANNNI model is more justified in case of stacking faults with nearly undistorted local atomic geometries (such as the I_1) when the SFE can be expressed in terms of interlayer interaction energies, while different approaches are needed for generalized SFE calculations with highly distorted local atomic geometries (see, e.g., [19, 20]).

Further, relative volumes changes due to alloying are defined as:

$$\Delta V\left(\mathrm{Mg}_{15}X\right) = V\left(\mathrm{Mg}_{15}X\right) - V\,(\mathrm{Mg16}) \tag{4}$$

and the relative change of the SFE due to alloying as:

$$\Delta I_1\mathrm{SFE}\left(\mathrm{Mg}_{15}X\right) = I_1\mathrm{SFE}\left(\mathrm{Mg}_{15}X\right) - I_1\mathrm{SFE}(\mathrm{Mg}). \tag{5}$$

Here, Mg is taken as the reference (ΔV(Mg) = 0 and ΔI$_1$ SFE(Mg) = 0).

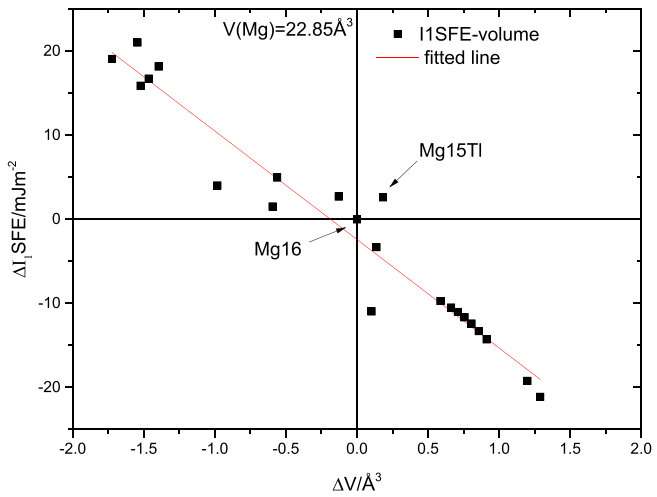

Figure 2. Relative change of the stacking fault energy Δ I_1 SFE of $Mg_{15}X$ as a function of the change of volume per atom in a Mg-alloy Δ V ($Mg_{15}X$). The data-points can be divided into two groups by the atomic volume of pure Mg (22.85 Å^3). All RE-elements increase the volume of $Mg_{15}X$ alloys. Almost all non-RE elements reduce the $Mg_{15}X$ volumes, with Tl being an exception.

The I_1 SFEs of 18 different Mg alloys were calculated including 8 RE solutes (RE = Er, Ho, Lu, Sc, Tm, Nd, Pr, Y) and 10 non-RE elements (non-RE = Co, Os, Tc, Tl, Be, Re, Ru, Ti, Zr and Zn). As the applied method based on the ANNNI model was validated particularly for hcp and dhcp metals, lanthanides with other crystal structures (Ce, Pm, Sm, Eu, and Yb) were not considered. Since the PAW pseudopotentials available in the VASP database cannot correctly predict the ground state of Gd, Tb and Dy, we have not considered them either.

3. Results and discussion

3.1. Five groups of relationships

3.1.1. Relation between ΔI_1 SFE($Mg_{15}X$) and volumes

First we analyzed the relation between the I_1 SFE and the volume per atom in $Mg_{15}X$ alloys. Figure 2 shows the computed ΔI_1 SFEs as a function of the relative atomic volumes of these alloys. Generally, the I_1 SFE is lower when the volume of the alloy is larger. This strong anti-correlation between ΔI_1 SFE($Mg_{15}X$) and $\Delta V(Mg_{15}X)$ can be mathematically expressed by a Pearson correlation coefficient $r = -0.97$. Mg-RE alloys have a larger atomic volume than pure Mg, and thus they lower the I_1 SFE with respect to pure Mg. The ΔI_1 SFE($Mg_{15}X$) values for elements of the lanthanide series are very close to each other, probably because they share a similar electronic structure. Mg-Y deviates from this pronounced trend. When comparing Y and Sc, Mg-Y has a smaller volume than Mg-Sc, but a lower ΔI_1 SFE($Mg_{15}X$) than Mg-Sc (that is 50% higher). One origin of this difference may lie in their electronic structures. Scandium and yttrium belong to the same group (IIIB group) as the lanthanide series elements, but they are in different periods and, consequently, have different outer electron shells. The electrons in these atomic shells may account for the differences in the I_1 SFE. The relation between the I_1 SFE and the period number will be discussed in detail below.

Almost all Mg-alloys containing non-RE solutes have negative $\Delta V(Mg_{15}X)$ values and positive ΔI_1 SFE ($Mg_{15}X$) values. The only exception is Tl; $Mg_{15}Tl$ has a larger volume than Mg and also higher I_1 SFE than Mg. As the non-RE elements are from different groups and periods, they share hardly any similarity in their electronic structures. Therefore the data points of Mg-non-RE alloys are more scattered around the interpolating line. Importantly, we can conclude that the volume per atom in Mg alloys is strongly anti-correlated with its I_1 SFE and the atomic volume of alloys is a reliable indicator of the SFE changes. The question is if we can further connect the volumetric changes in alloys with the atomic volume of pure solutes.

Having the SFE in Mg-alloys related to the atomic volume in these alloys, we further analyze the latter as a function of the atomic volume of elemental solutes. Figure 3 shows the relation between the atomic volume of a solute X and the average atomic volume V of $Mg_{15}X$ alloys. It is worth mentioning that DFT methods usually predict the lattice parameters very accurately with only very small deviations from experimental data. Here both volumes are derived from *ab initio* calculations. The values follow a rather intuitive trend: when a larger atom X is placed into a $Mg_{15}X$ supercell, the average atomic volume of the alloy increases. Most of the elements considered follow this trend. The high Pearsons correlation coefficient $r = 0.95$ indicates a strong correlation between the elemental volume and the alloy volume. Nevertheless, there are exceptions from this rule. For example, elemental zirconium (Zr) is larger than Mg, but the atomic volume of $Mg_{15}Zr$ is smaller than the

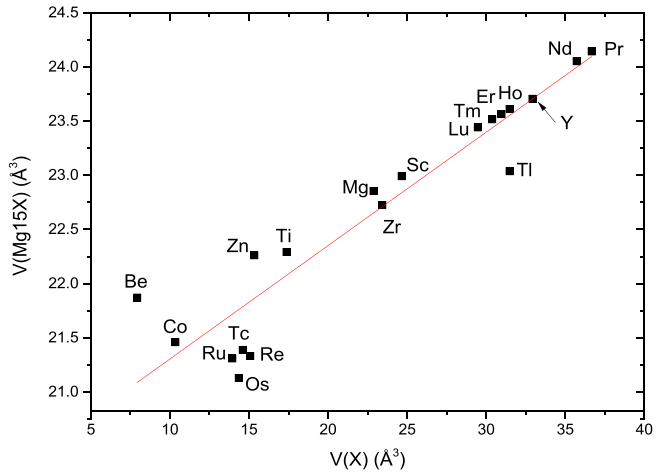

Figure 3. Relation between $V(Mg_{15}X$, per atom) and volume $V(X$, per atom). The data-points mostly follow a linear trend: a larger atomic volume of X correlates with a larger averaged atomic volume of $Mg_{15}X$.

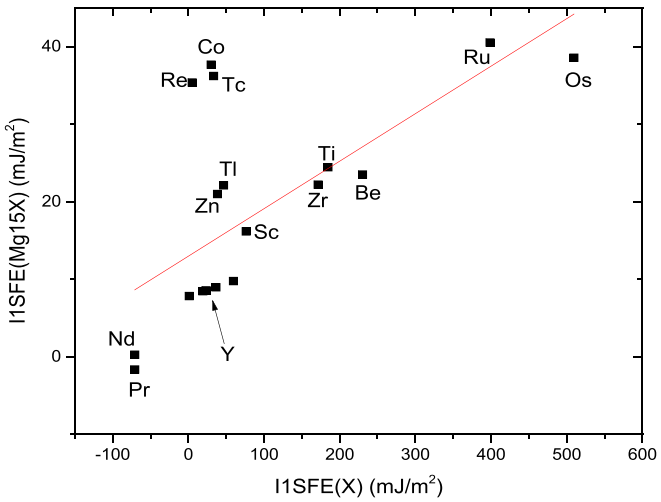

Figure 4. Relation between the I_1 SFE of $Mg_{15}X$ alloy and the I_1 SFE of elemental X.

volume of both pure Zr and Mg. Another exception is Tl. The volume of Tl is 30% larger than Mg, but when incorporated into the Mg matrix it changes less than 1% of the average volume of Mg_{15} Tl. We assume that strong chemical bonds are formed between Mg atoms and these solutes (e.g. Zr, Tl) and subsequent electron transfers lead to this anomaly. In the non-RE group, Tc, Ru, Re and Os deviate slightly from this linear trend. These four transition metals have approximately the same volume and all significantly reduce the atomic volume of $Mg_{15}X$ (which is even smaller than that in Mg_{15} Be). The contracted volumes also indicate formation of strong chemical bonds.

3.1.2. I_1 *SFEs in pure solutes and Mg alloys*

Figure 4 shows the relation between the I_1SFEs in (i) $Mg_{15}X$ alloys and (ii) pure solutes X. The SFE of $Mg_{15}X$ increases slowly with the SFE of pure X but a clear linear trend is not evident. Still, the increasing trend can be interpreted such that if an I_1SF is energetically difficult to be generated in a metal X, so it is in the $Mg_{15}X$ alloy. The points can be fitted to a linear relation but the corresponding correlation coefficient, $r = 0.67$, is rather low. The linear fit equation reads (unit in mJ m^{-2})

$$\gamma\left(Mg_{15}X\right) = (0.061 \pm 0.015)\ \gamma(X) + (12.96 \pm 2.45). \tag{6}$$

Interestingly, the slope is $0.061 \pm 0.015 \approx 0.0625 = 1/16$, which is exactly the atomic concentration of element X in $Mg_{15}X$. However an approximation based on the fractional concentrations is only roughly indicative. Among the studied elements, Re, Co, and Tc possess medium-level SFEs but when added into $Mg_{15}X$ supercells,

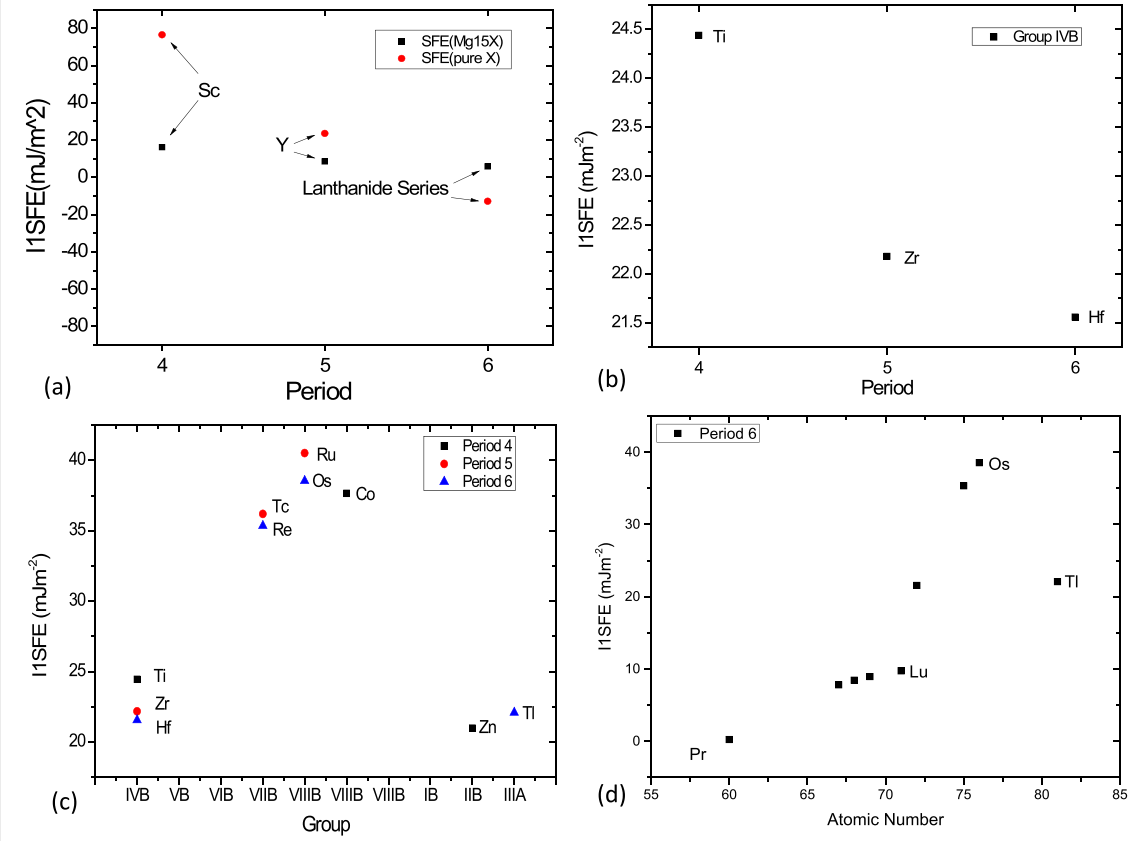

Figure 5. The I_1SF energies as functions of the period number (a,b), the group number (c) and the atomic number (d).

the corresponding alloys have rather high SFEs (≈35 mJ m^{-2}). In an opposite manner, the SFE of rhenium is significantly lower (5 mJ m^{-2}) than that in Mg_{15} Re (35 mJ m^{-2}).

The negative SFEs of Mg-*X* alloys (*X* = Nd, Pr) can be understood in such a way that the I_1SF can form energetically spontaneously, and there is no extra energy needed to obtain I_1SF in the alloys. In the ANNNI model, the I_1 SFE is proportional to the term (E_{dhcp}—E_{hcp}), i.e., the total energy difference between the phases with hcp and dhcp stacking sequences. When I_1 SFE is negative, $E_{dhcp} < E_{hcp}$, the alloy is more energetically stable in a dhcp structure than in the hcp one.

3.1.3. I_1 *SFEs and the atomic number of solutes*

The lanthanide elements have similar affinities and chemical properties which is a result of similar atomic and electronic structures, and they are often visualized in the periodic table of elements as a single element. Therefore we have defined an average I_1 SFE for the considered lanthanide elements. The I_1 SFEs as a function of period are shown in figure 5(a) and (b). The I_1 SFEs of elemental RE and non-RE solutes decrease with increasing periodic number, but the slope levels down for higher periodic numbers. A similar trend is predicted also for the respective $Mg_{15}X$ (*X* = RE) alloys but with a smaller slope.

All ten Mg-non-RE alloys considered, which belong to three different periods, are shown as function of group number (see figure 5(c)). The I_1 SFEs of $Mg_{15}X$ of these alloying elements increase when moving from group IVB to VIIIB and decrease from group VIIIB to IIIA (see the values for periods 4 and 6). Figure 5(d) shows the I_1 SFE of five RE elements and four non-RE elements in Period 6. From Pr to Os, the I_1 SFE values increase with the atomic number but then they decrease (see the data point for Tl). The increasing rate from Lu to Os is higher compared to that from Pr to Lu.

If we do not collapse all lanthanides into a single data point but visualize them separately, the I_1 SFEs of lanthanides are shown in figure 6. The I_1 SFE values grow as a function of the atomic number within the lanthanide series in case of both elemental solutes and Mg-alloys containing them. The two trends in I_1 SFEs as a function of the atomic number (lanthanides and Mg-alloys) are different and, therefore, they are individually depicted in figures 6(a) and (b). The I_1SF energies in pure solutes grow in a concave manner as a function of the atomic number (figure 6(a)) while for $Mg_{15}X$ alloys, the I_1 SFE values first increase in a convex manner and then increase in a concave manner for higher atomic numbers (figure 6(b)). Fortunately, both trends deviate from linear trends only very weakly and so correlations are not significantly reduced.

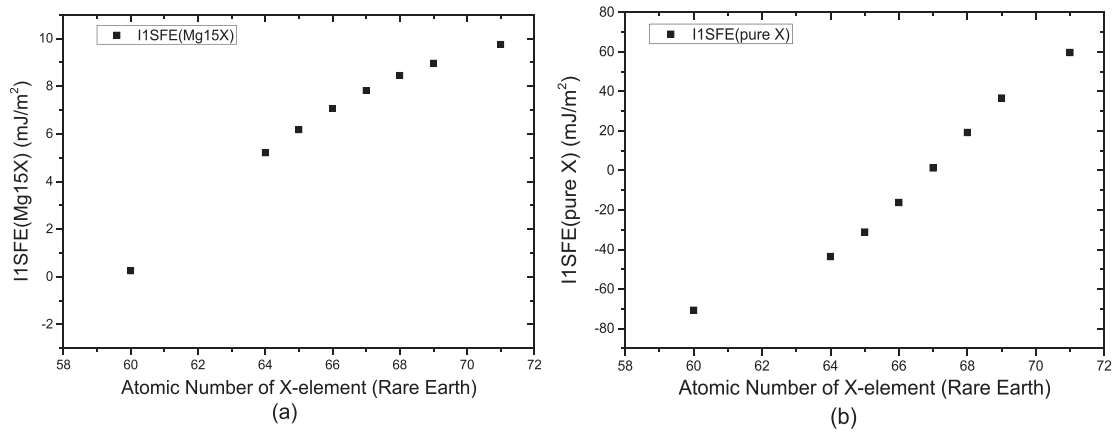

Figure 6. I_1 SFE in (a) $Mg_{15}X$ alloys (X = RE elements) and (b) elemental Sc, Y and lanthanides as function of the atomic number of element X.

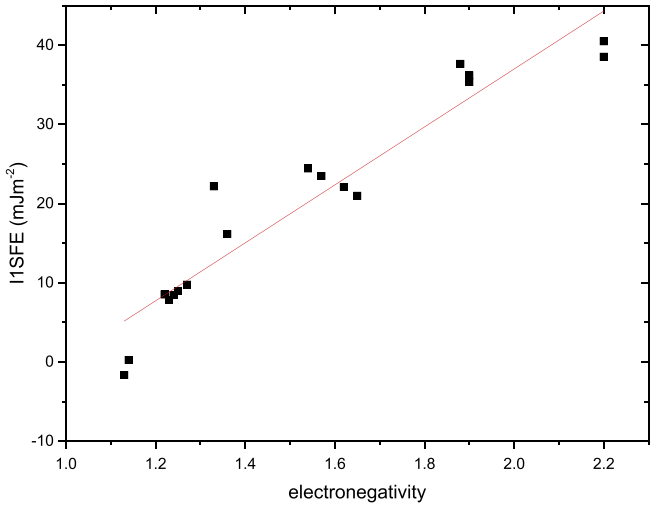

Figure 7. Relation between the I_1 SFE in $Mg_{15}X$ alloys and the electronegativity of different solute elements X.

3.1.4. I_1 *SFEs and electronegativity*

The I_1 SFEs computed for different binary Mg alloys as a function of the electronegativity of the individual alloying elements are depicted in figure 7. The data for the electronegativity have been taken for all solutes considered (both RE and others) from [32]. Even though some local trend (e.g. the four elements around 1.6 electronegativity) is seen, globally the values of I_1 SFE in $Mg_{15}X$ increase with increasing electronegativity of elemental solutes. The data points seem to be strongly correlated and the corresponding Pearsons correlation coefficient, $r = 0.95$, is very high. The electronegativity is an excellent linear indicator of SFE changes induced by alloying.

3.1.5. I_1 *SFEs and bulk modulus*

Figure 8 shows the relation between the I_1SF energies in $Mg_{15}X$ alloys and the value of the bulk modulus of solute elements. The bulk moduli are calculated for all metals considered at their ground state structure, i.e. dhcp crystals in the case of Pr and Nd and hcp crystals for all other considered metals. The I_1SF energies in $Mg_{15}X$ alloys clearly grow with the bulk modulus computed for the elemental solutes but the trend visible in figure 8 is not a simple linear function. We propose a logarithmic relation between both quantities, as it seems to fit better and gives a rather high correlation coefficient $r = 0.90$. In linear fitting, this coefficient is 0.87. The bulk modulus is thus a good logarithmic indicator of I_1 SFE changes upon alloying.

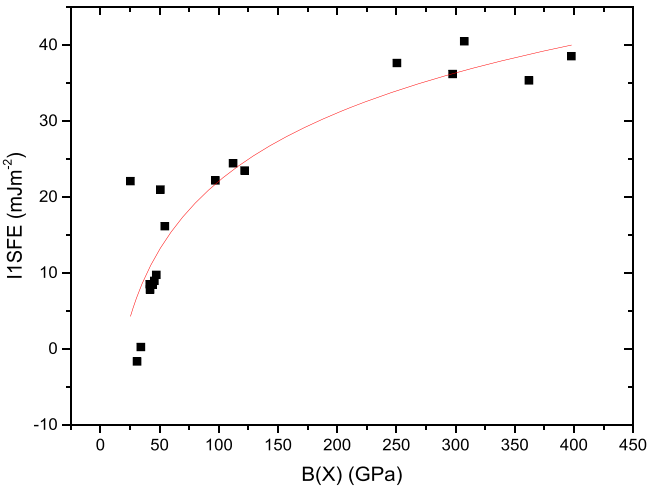

Figure 8. Relation between the I_1 SFE ($Mg_{15}X$) and the bulk modulus of element X.

3.2. YSI of binary Mg alloys

We have studied five separate dependencies between the I_1 SFEs of Mg alloys on the one hand and various materials characteristics of elemental solutes on the other. We find that three of them possess strong correlations or anti-correlations with the I_1SF energies, specifically, (i) the atomic volume; (ii) electronegativity; and (iii) the bulk modulus. The corresponding Pearsons correlation coefficients are −0.97, 0.95 and 0.90, respectively. Interestingly, the I_1SF energies are found to be (anti-) correlated to (i) the volume, i.e., a structural characteristic, (ii) the electronegativity which is an electronic structures property, and (iii) the bulk modulus, one of the elastic parameters. Similar mutual (anti-) correlations were previously found also in other systems. For example, in the case of body-centered-cubic Fe-Ti alloys, their thermodynamic stability (expressed in terms of their formation energies) were found to be strongly related to their density of state at the Fermi level (an electronic structure characteristics). Furthermore, each of these properties (the formation energy and the density of states) were found to be strongly (anti-) correlated with the polycrystalline Youngs modulus of these alloys [33]. Other (anti-) correlations between the thermodynamic stability and elastic parameters were found in face-centered-cubic alloys e.g. Ni-W [34] or Ni nitrides [35]. Apparently, such relations between the atomic-scale electronic structure parameters and macro-scale properties are rather independent on the actual crystal structure and material system.

A comparison of the above discussed parameters is presented in figure 9, where all elements are sorted according to their (a) atomic radius, (b) electronegativity and (c) bulk modulus. From figure 9 it is evident that all elements which reduce the I_1 SFE in Mg (lanthanides, Y, Sc) have (i) large atomic radii of $\geqslant$ 184 pm (Mg: 145 pm), (ii) electronegativity values close to the that of Mg (1.1–1.3) and (iii) bulk moduli close to Mg, i.e. 32-56 GPa (see our recent paper [8] for further details). A more detailed analysis of these parameters shows that Sc, which only moderately reduces the I_1 SFE in Mg, fulfills all three criteria but its values are a bit away from those of Y and the lanthanides. Additionally, it was revealed that none of the other elements (i.e. others than lanthanides, Y and Sc) fulfills all three criteria.

Having all these above discussed findings we see that there are three critically important parameters of solutes (the atomic volume, electronegativity, and the bulk modulus) that should be considered. As it is rather inconvenient to simultaneously consider multiple criteria, we below attempt to provide a single evaluation factor integrating all three parameters. Due to the fact that we aim at ductility improvements, we use yttrium as a reference below because it is known to improve the ductility of Mg alloys [2, 4, 5]. Below we thus compare properties of other solutes with those known for Y. Based on the above summarized relations we define an YSI, a new numerical indicator which combines the atomic volume, electronegativity and the bulk modulus. We define the YSI as follows

$$\mathrm{YSI}_i = 1 - \sqrt{w_v\left(v_i - v_Y\right)^2 + w_\nu(\nu_i - \nu_Y)^2 + w_B\left(B_i - B_Y\right)^2}, \tag{7}$$

where i = H, Li, Be, ...Bi. The quantities v, ν and B represent the atomic volume, electronegativity and the bulk modulus of an element, respectively, and w_v, w_ν and w_B are the weights of the three components. Their values are determined by the slopes of their linear fitting equations and normalized by setting the maximal YSI_i as 1. Under these conditions, $(w_v, w_\nu, w_B) = (1.887, 1.777, 0.511)$. The three components enter this equation normalized by the largest values of the selected 76 elements from the periodic table of elements, namely the atomic volume of

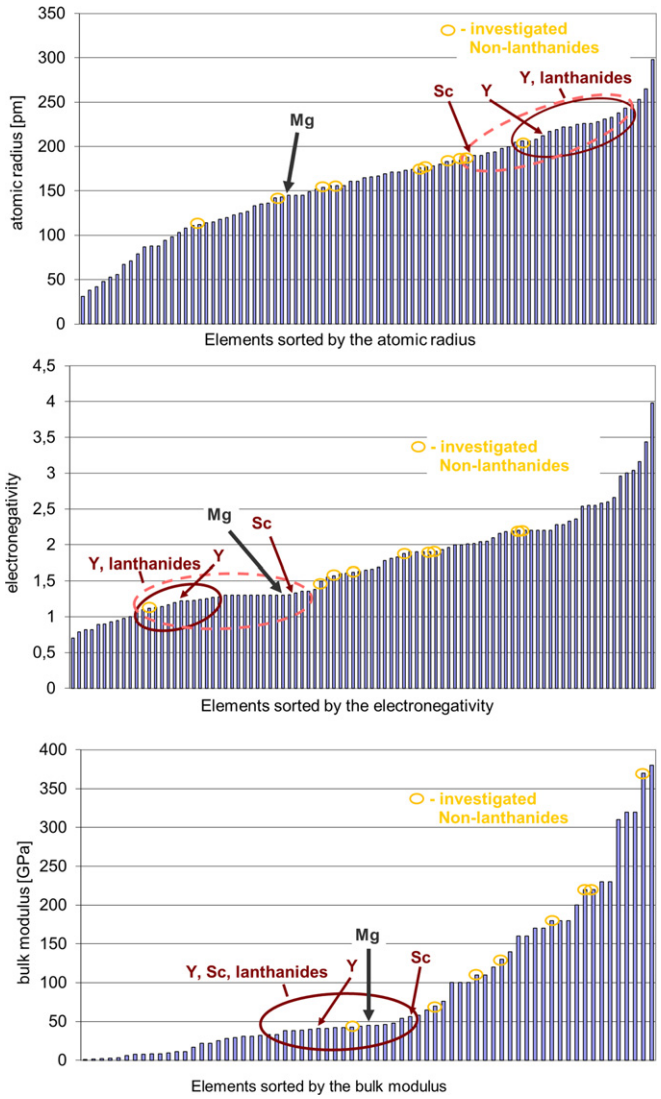

Figure 9. Selected 76 elements from the periodic table sorted by their (a) atomic radius, (b) electronegativity and (c) bulk modulus [32]; the lanthanides, Y and Sc have (i) large atomic radii of $\geqslant$ 184 pm (Mg: 145 pm), (ii) electronegativity values close to the that of Mg (1.1–1.3) and (iii) bulk moduli close to Mg (32–56 GPa); none of the other elements have all three parameters in the same range; the elements which were considered in the present study and calculated to increase the I_1 SFE are shown by yellow circles. The pink dash-line circles the lanthanide series and Sc, Y.

Cs (117 Å^3), the electronegativity of F (3.98), and the bulk modulus of Os (462 GPa). As the reference, the atomic volume, electronegativity and bulk modulus of yttrium are 33 Å^3, 1.22 and 41 GPa. The YSI parameter defines a specific metric or 'distance' between an element and yttrium in a property space. The larger YSI is, the more similar it is to yttrium. It should be noted that the YSI is introduced as a concentration-independent quantifier because it compares only concentration-independent materials characteristics of elemental solutes with corresponding values that are known for pure yttrium. The fact that most of I_1SF energies discussed in our study were computed for one specific solute concentration (6.25 at.%) is therefore of only limited importance.

The three selected characteristics of 76 elements from the periodic table of elements are together with their computed YSI values summarized in table 1. For the lanthanide series (from Ce to Lu), the YSI values are very large and close to each other. By using the YSI we can identify the lanthanide elements as the most similar elements to yttrium (see table 2). That matches the above discussed I_1 SFEs which are low for Mg-RE binaries. The non-RE elements with the highest YSI values (0.84–0.86) are Na, Ca, Zr, Tl, and Li. Judging from their YSI values which are very close to Mg (0.84), these non-RE elements do not guarantee a reduction of the I_1 SFE in Mg alloys since our model is based on an approximation of three (anti-)correlations. Calcium was found to decrease the elongation of Mg up to a concentration of 3 wt% [37]. Salahshoor *et al* performed a more dense set of experiments on samples with 0–4.0 wt% of Ca [38]. They found that Ca could increase the elongation of Mg by 4% for an alloying content of up to $\approx$ 0.5 wt% but decreases the elongation for higher concentrations. There are,

Table 1. Parameters characterizing solute elements ('El.'), the electronegativity ν (by Pauling scale), bulk modulus B and atomic volume V (as taken from [32] and [36]), together with the computed yttrium similarity index (YSI) values. It is noted that usually interstitial elements (such as H, B, C, N, O or F) are here treated as substitutional.

El.	ν	B (GPa)	V (Å^3)	YSI	El.	ν	B (GPa)	V (Å^3)	YSI
H	2.2	41	1.19	0.504	Ru	2.2	220	13.60	0.514
Li	0.98	11	21.50	0.837	Rh	2.28	380	13.70	0.328
Be	1.57	130	8.09	0.657	Pd	2.2	180	14.70	0.553
B	2.04	320	7.30	0.406	Ag	1.93	100	17.10	0.684
C	2.55	33	8.83	0.472	Cd	1.69	42	21.60	0.793
N	3.04	41	1.40	0.287	In	1.78	41	26.10	0.796
O	3.44	41	0.89	0.167	Sn	1.96	58	27.00	0.741
F	3.98	41	0.59	0.001	Sb	2.05	42	30.20	0.720
Na	0.93	6.3	39.50	0.866	Te	2.1	65	34.00	0.703
Al	1.61	76	16.60	0.761	I	2.66	7.7	42.70	0.502
Si	1.9	100	20.00	0.711	Cs	0.79	1.6	117.00	0.000
P	2.19	11	28.20	0.667	Ba	0.89	9.6	65.00	0.607
S	2.58	7.7	27.20	0.537	La	1.1	28	37.50	0.931
Cl	3.16	1.1	3.94	0.264	Ce	1.12	22	34.80	0.951
K	0.82	3.1	75.90	0.478	Pr	1.13	29	35.30	0.956
Ca	1	17	43.00	0.858	Nd	1.14	32	34.20	0.967
Sc	1.36	57	25.00	0.892	Sm	1.17	38	34.00	0.979
Ti	1.54	110	17.60	0.765	Eu	1.2	8.3	48.10	0.816
V	1.63	160	13.80	0.679	Gd	1.2	38	33.10	0.992
Cr	1.66	160	12.10	0.660	Tb	1.2	38.7	32.10	0.987
Mn	1.55	120	12.20	0.706	Dy	1.22	41	31.60	0.983
Fe	1.83	170	11.80	0.621	Ho	1.23	40	31.20	0.978
Co	1.88	180	11.00	0.598	Er	1.24	44	30.60	0.971
Ni	1.91	180	10.90	0.592	Tm	1.25	45	30.10	0.964
Cu	1.9	140	11.80	0.630	Yb	1.1	31	43.80	0.867
Zn	1.65	70	15.20	0.743	Lu	1.27	48	29.50	0.955
Ga	1.81	41	19.60	0.748	Hf	1.3	110	22.30	0.833
Ge	2.01	75	22.70	0.704	Ta	1.5	200	18.10	0.684
As	2.18	22	21.70	0.651	W	2.36	310	15.90	0.401
Se	2.55	8.3	27.20	0.547	Re	1.9	370	14.70	0.403
Br	2.96	1.9	42.50	0.404	Os	2.2	462	14.00	0.237
Rb	0.82	2.5	92.70	0.287	Ir	2.2	320	14.20	0.415
Sr	0.95	41	55.30	0.724	Pt	2.28	230	15.40	0.496
Y	1.22	41	33.00	1.000	Au	2.54	220	17.00	0.446
Zr	1.33	91.1	23.30	0.857	Hg	2	25	24.60	0.720
Nb	1.6	170	18.00	0.705	Tl	1.62	43	28.70	0.857
Mo	2.16	230	15.50	0.524	Pb	2.33	46	30.40	0.627
Tc	1.9	41	14.20	0.683	Bi	2.02	31	35.50	0.730

Table 2. Statistical data of YSI values. Yttrium has the maximum value of the YSI and Cs the minimum one.

Average YSI	0.66
Maximum YSI	1
Minimum YSI	0
Top ten elements	Y, Gd, Tb, Dy, Sm, Ho, Er, Nd, Tm, Pr
Lowest ten elements	Cs, F, O, Os, Cl, N, Rb, Rh, W, Re
Top five of non-RE	Na, Ca, Zr, Tl, Li

unfortunately, no experimental data for Mg-Na alloys available. The solubility of Na in Mg is very low (see Mg-Na phase diagram), therefore Na is not a promising solute of interest. Zirconium has a too low solubility in Mg, hence it is used as a grain refiner [39]. No data for Mg-Tl alloys are available. Li is a well-known solute that can improve the ductility of Mg [40–43] by enhanced activity of $\langle c + a \rangle$ dislocations [43], which is consistent with our prediction.

There are no bulk modulus data available for H, N, O, F, Ga, Tc and In. The bulk modulus term in the YSI determination is then ignored by setting $B_i = B_Y = 41$ GPa. However, it was found that these (mostly interstitial

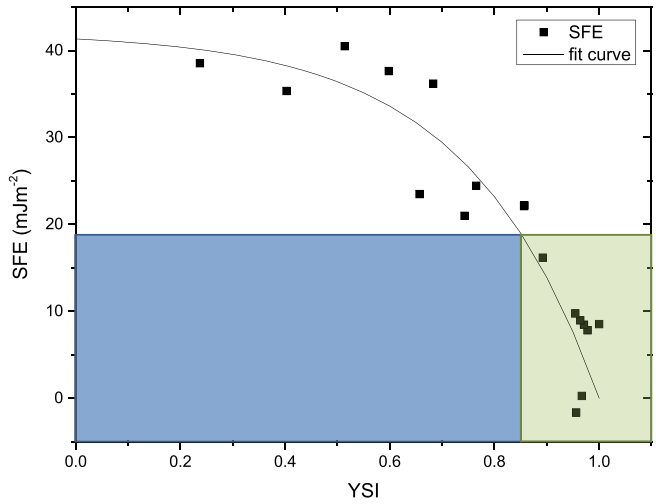

Figure 10. Relationship between SFE and YSI with the horizontal border line indicating the I_1 stacking fault energy value in pure Mg. Elements decreasing the I_1 stacking fault energy in Mg alloys are in the part with a greenish background.

elements that are here treated as substitutional) possess rather low YSI values, i.e. low similarity to Y (see table 2) and we do not expect them to reduce the energy of I_1SF by substituting Mg atoms.

We show the relation between the I_1SFE and YSI for 18 Mg alloys in figure 10. The SF energies decrease with increasing YSI. At low YSI values the I_1 SFE decreases slowly, then the falling slope of the I_1SFE increases and finally the I_1SFE drops rather sharply for high YSI values. This relation can be fitted to an exponential function as

$$\gamma = 42.11(1 - \exp\{4(\mathrm{YSI} - 1)\}) \quad \left(\mathrm{mJ\,m^{-2}}\right) \tag{8}$$

which is characterized by a high Pearson correlation coefficient $r = 0.93$. The exponential character of the trend in figure 10 is partly due to the logarithmic relation between the bulk moduli and the I_1 SFEs. In our definition of the YSI, we use linear functions (concept of distances in a generalized space of materials properties of elements). By using this exponential function we can easily find the lowest values of the YSI parameter that leads to a reduction of the I_1 SFE in Mg alloys (compared with elemental Mg). This critical value is associated with the I_1 SFE of pure Mg (19.47 mJ m^{-2}), and the threshold value of YSI is 0.84 ($\approx 1 - 1/4 \ln 2$). In figure 10. Therefore, the elements which can possibly reduce I_1SFEs are expected to have the YSI values above 0.84 and the I_1SFE lower than 19.47 mJ m^{-2}. For elements with YSI $\geqslant$ 0.84, their locations in the properties space are shown in figure 11 (some elements with YSI smaller than 0.84 are also shown).

Our findings can be interpreted as sever fundamental limitations in any search for alternative solutes ductilizing magnesium (there is only a single non-RE element, Li, having a YSI $\geqslant$ 0.84). Consequently, alloy-design strategies should be rather focused on multi-component alloying concepts (e.g., ternary or quaternary Mg-alloys) that can potentially provide a necessary reduction of the I_1SFE as yttrium by combining more than one solute. In order to pave this way, we below extend our searching space of solutes from binaries to ternaries and demonstrate the performance of our screening and search method.

3.3. YSI and I_1 SFE of ternary Mg alloys

3.3.1. Extending the concept of YSI to ternaries

The YSI concept introduced above (see equation (7) is based on comparing selected materials properties of individual solutes to corresponding materials properties in yttrium with the aim to identify individual solutes. In case of Mg-based ternaries containing two different solutes at once, we would like to assign a single numerical evaluator to a pair of solutes, each of them having different elemental materials properties.

In order to extend the YSI concept to multi-component alloys, we propose to use solute-ratio weighted averages of materials parameters of individual solutes, i.e., averages of materials properties of both individual participating solutes in case of two solutes with an equal atomic-percent amount (see the cases discussed below). In the ternary case we then re-write the YSI formula for a single solute (equation (7)) and extend the YSI concept to ternary Mg alloys as follows

$$\mathrm{YSI}_{ij} = 1 - \sqrt{w_\nu\left(\nu_{ij} - \nu_Y\right)^2 + w_\nu(\nu_{ij} - \nu_Y)^2 + w_B\left(B_{ij} - B_Y\right)^2}, \; i \neq j. \tag{9}$$

$i, j =$ H, Li, Be, ...Bi, using averaged materials parameters, the atomic volume $\nu_{ij} = (\nu_i + \nu_j)/2$, the bulk modulus $B_{ij} = (B_i + B_j)/2$, and the electronegativity $\nu_{ij} = (\nu_i + \nu_j)/2$, weighted by the same weights w_ν, w_e

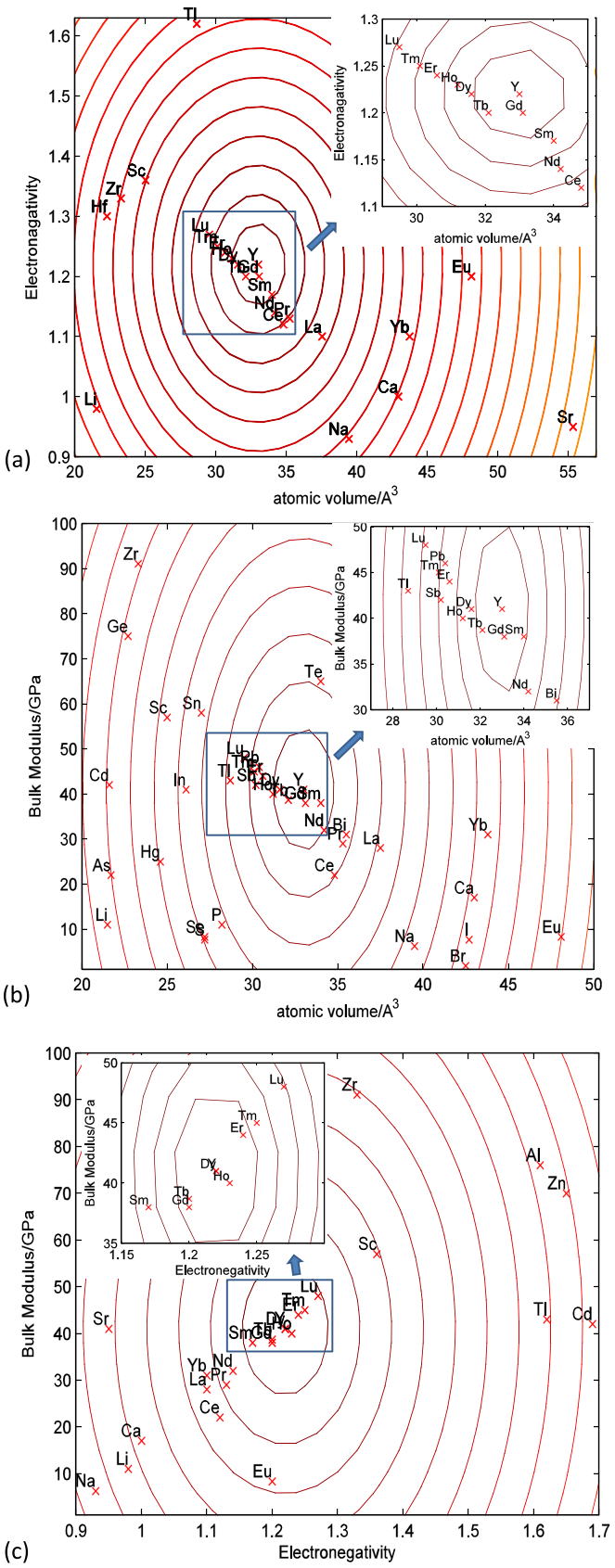

Figure 11. Selected elements with YSI values $\geqslant 0.84$ projected onto plane with different property pairs: (a) atomic volume and electronegativity; (b) atomic volume and bulk modulus; and (c) electronegativity and bulk modulus. Whenever datapoint symbols and their legends overlap, an inset shows a suitable magnification.

Table 3. The statistic data of YSI values computed for Mg-based ternaries. Since our aim is to find non-RE solute pair that have high YSI, only data for pairs that do not contain RE elements are listed.

YSI	No. of combinations
$0.85 \leqslant$ value<0.95	122
$0.95 \leqslant$ value<0.98	11
$0.98 \geqslant$ value	0

Table 4. Yttrium similarity index (YSI) for 133 non-RE solute pairs with YSI larger than 0.85. Among them 11 solute combinations possess YSI larger than 0.95.

Solutes	YSI	Solutes	YSI	Solutes	YSI	Solutes	YSI	Solutes	YSI
Fe,K	0.851	Te,Ca	0.872	Bi,Li	0.888	Sr,Cr	0.903	Sr,Be	0.928
Ba,Ge	0.852	Zr,Li	0.873	Sb,Ca	0.888	Sb,Na	0.904	Tc,Sr	0.929
Sb,Sr	0.852	Ba,Si	0.873	Ba,H	0.888	V,Ca	0.904	Zn,Na	0.930
Zn,K	0.853	Sr,Co	0.874	Nb,Sr	0.890	Ge,Ca	0.904	Ga,Na	0.930
Cu,K	0.857	Tl,Zr	0.875	Cr,Na	0.890	Ba,Cr	0.905	Ga,Ca	0.932
Cr,K	0.857	Fe,Na	0.875	Ta,Ca	0.891	Tc,Ca	0.905	Sr,Ti	0.932
Cd,Li	0.859	P,Na	0.875	Sr,Li	0.891	Ag,Sr	0.906	Sr,Mn	0.937
Pb,Na	0.859	Ba,Nb	0.875	Ba,Fe	0.891	Ag,Ca	0.907	In,Ca	0.938
Ta,Ba	0.860	Ba,Cd	0.875	Te,Na	0.892	Hf,Sr	0.908	Ba,Be	0.939
Ni,Na	0.861	Sn,Sr	0.876	Ta,Na	0.892	Ag,Na	0.908	Al,Na	0.939
Ni,Ca	0.862	Bi,Ca	0.876	Tl,Sr	0.893	Hg,Na	0.908	Ti,Na	0.941
Co,Na	0.864	Te,Li	0.876	Na,Li	0.894	Ba,Al	0.909	Zn,Ca	0.942
Ca,Na	0.864	Fe,Ca	0.877	Bi,Na	0.894	Mn,Na	0.909	In,Na	0.947
Hf,Li	0.864	As,Na	0.877	Cr,Ca	0.896	Nb,Ca	0.910	Hf,Na	0.949
Ca,P	0.864	In,Li	0.877	Sr,Cu	0.897	Sn,Ca	0.910	Ti,Ca	0.950
Ba,Zr	0.864	K,H	0.880	Ca,Be	0.897	Nb,Na	0.910	Cd,Na	0.951
Co,Ca	0.865	Ba,Ga	0.881	In,Sr	0.898	Ca,Li	0.912	Sr,Al	0.952
Hf,Ba	0.866	Hg,Sr	0.881	Ba,V	0.898	Zr,Sr	0.913	Ca,Al	0.952
Mn,K	0.867	Cu,Na	0.881	Tc,Na	0.899	Ge,Na	0.913	Tl,Ca	0.952
Sr,As	0.867	Ba,Ni	0.882	Ba,Ti	0.899	Ba,Zn	0.915	Cd,Ca	0.954
Sn,Li	0.867	Cu,Ca	0.884	Ba,Cu	0.899	Ca,Si	0.916	Sr,Zn	0.956
Sb,Li	0.869	Na,Be	0.884	V,Na	0.899	Mn,Ca	0.922	Hf,Ca	0.958
Sr,H	0.869	Ba,Co	0.884	Hg,Ca	0.901	Si,Na	0.922	Zr,Na	0.962
Tl,Hf	0.869	Sr,Fe	0.885	Ba,Tc	0.901	Sn,Na	0.923	Tl,Na	0.966
Ta,Sr	0.870	Ba,Ag	0.885	Tl,Li	0.901	Ba,Mn	0.925	Zr,Ca	0.973
As,Ca	0.871	Sr,Ge	0.885	Sr,Si	0.901	Sr,Ga	0.925		
Sr,Ni	0.871	K,Be	0.887	Sr,V	0.903	Cd,Sr	0.928		

and w_B as in equation (7). The total number of solutes pairs (containing two different solutes) is $76 \times 76/2 - 76 = 2850$.

Applying equation (9), the YSI values of all 2850 combinations were calculated. Since our aim is to identify solute pair that consists of non-RE elements but is also able to reduce the I_1 SFE like yttrium, the RE elements are excluded from our discussion of results below.

No non-RE candidates possess YSI above 0.98. The statistical data of the matrix are listed in table 3. There are 133 non-RE solute pairs witha YSI larger than 0.85. These solute candidates along with their YSI are listed in table 4 ordered according to their YSI value from the lowest to the highest one. The last 11 solute pairs in table 4 have YSI values larger than 0.95. Except (Sr,Zn), ten of these pairs contain either Ca, Na or Al. Among these ten pairs, five solute pairs contain Ca, three include Na and two contain Al.

3.3.2. Ab initio computed SFEs in Mg-based ternaries

In order to test the reliability of the above predictions of solute pairs based on the YSI, we below determine the I_1 SFEs for 11 promising solute pairs from the ANNNI model. To do so, quantum-mechanical calculations have been performed for supercells with two non-equivalent configurations of two solutes in both hcp and dhcp supercells (shown in figure 1). The solutes are located so as to maximize their mutual distances within the supercells. The chosen arrangements minimize their mutual interactions as expected in case of low and dilute concentrations. Minimum interactions between solute atoms are also in line with our proposed extension of the

Table 5. The *ab initio* computed I_1 SFEs of ternary Mg alloys with solutes consisting of only non-RE elements with YSI larger than 0.95. The I_1SF energies were computed using the ANNNI model from the four energies of hcp and dhcp supercells depicted in figure 1. They are noted as '1-1', '1-2', '2-1', and '2-2' when, e.g., '1-2' means the I_1 SFE is computed from the energy difference of $E_{\mathrm{dhcp}-1}$ and $E_{\mathrm{hcp}-2}$. The unit of the numbers is mJ m^{-2}. The last column contains a verbal evaluation of the potential of listed solute pairs with respect to the reduction of I_1 SFE in Mg-based ternaries.

Solutes	YSI	1-1	1-2	2-1	2-2	Minimum	Average	Potential
Ti,Ca	0.950	26.9	16.4	17.8	7.3	7.3	17.1	Very promising
Cd,Na	0.951	18.2	21.1	20.0	23.3	18.2	20.7	Promising
Sr,Al	0.952	9.1	18.2	17.5	26.2	9.1	17.8	Very promising
Ca,Al	0.952	14.6	19.3	20.0	24.7	14.6	19.6	Promising
Ca,Al[a]	0.952	13.8	18.6	19.3	24.0	13.8	18.9	Very promising
Tl,Ca	0.952	15.6	18.9	16.7	20.0	15.6	17.8	Very promising
Cd,Ca	0.954	15.6	20.0	18.6	22.9	15.6	19.3	Promising
Sr,Zn	0.956	13.1	18.9	18.6	24.7	13.1	18.9	Very promising
Hf,Ca	0.958	31.3	15.6	17.1	1.5	1.5	16.4	Very promising
Zr,Na	0.962	24.7	16.0	17.5	8.7	8.7	16.7	Very promising
Tl,Na	0.966	17.5	19.3	17.8	19.3	17.5	18.6	Very promising
Zr,Ca	0.973	40.0	27.7	7.3	−5.1	−5.1	17.5	Very promising

[a] Computed with the optimized lattice parameters $a = 3.199$Å, $c/a = 1.626$ (see the text for details).

YSI to ternaries and higher-component alloys when we use materials properties of individual solutes (see equation (9)).

For the four supercells we denote the total energies as $E_{\mathrm{hcp}-1}$, $E_{\mathrm{hcp}-2}$, $E_{\mathrm{dhcp}-1}$ and $E_{\mathrm{dhcp}-2}$. Due to the fact that the I_1SF energies are computed within the ANNNI model as the difference between energies of the hcp and dhcp structures, there are four I_1SF energies considered. These I_1SF energies are summarized in table 5 and noted as '1-1', '1-2', '2-1', and '2-2' when, e.g., '1-2' means that the I_1 SFE is computed from the energy difference of $E_{\mathrm{dhcp}-1}$ and $E_{\mathrm{hcp}-2}$. The '2-2' I_1SF energy is negative in case of the (Zr,Ca), i.e., the energy of the (Zr,Ca) pair in case of the dhcp-2 supercell is even lower than that in case of the hcp-2 supercell, and that would indicate that the stacking faults would form very easily, in fact spontaneously, if allowed by surrounding crystal matrix in this particular case.

At $T = 0$ K, the solutes choose their lattice position so as to minimize the energies (both in dhcp and hcp crystals) and the corresponding computed values of I_1 SFE are in table 5 in the 'min.' column (these I_1 SFE values are the smallest values among '1-1', '1-2', '2-1' and '2-2' combinations for each considered solutes pair). At finite temperatures, the solutes have non-zero probabilities to occupy also other positions, not only those that minimize the energy. As an estimate for the finite-temperature values of the I_1SF energies, we assume an equal probability for all crystal sites and compute an average value of the four I_1 SFEs and list them in table 5 in the column marked 'average'. We expect real values somewhere between the minimum value of the I_1 SFE and the average one. Therefore, we sort the solute pairs so that if both the minimum and averaged values are smaller than 19.47 mJ m^{-2} (the value found in the elemental Mg), the corresponding solute pair is considered as 'very promising' with respect to the reduction of the I_1 SFE in Mg ternaries. If only one of these two quantities is smaller than 19.47 mJ m^{-2}, the solute combination is considered as 'promising' to reduce I_1 SFE. Lastly, if both quantities are larger than 19.47 mJ m^{-2}, the candidate pair is evaluated as 'not promising' to reduce I_1 SFE.

Following the above explained evaluation, eight solute combinations, (Ti,Ca), (Sr,Al), (Tl,Ca), (Sr,Zn), (Hf, Ca), (Zr,Na), (Tl,Na) and (Zr,Ca), are predicted to be very promising with respect to reducing the I_1 SFE in Mg alloys. Three other solute pairs, (Cd,Na), (Ca,Al) and (Cd,Ca), are promising to reduce I_1 SFE of Mg. As seen, no solute pair was found 'not promising', i.e. unable to reduce the I_1 SFE in Mg alloys. That means an excellent agreement between our YSI-based prediction and benchmarking I_1 SFE quantum-mechanical calculations. The SFEs discussed above were computed using lattice constants of pure Mg ($a = 3.1886$Å, $c/a = 1.6261$). To assess an error introduced by this way of calculating the energies, the lattice constants of one specific solute pair (we choose Mg-(Al,Ca) as both Al and Ca are used as alloying elements in Mg alloys) were fully optimized and found equal to $a = 3.199$Å, $c/a = 1.626$. The subsequent use of the optimized lattice constants in our quantum-mechanical calculations resulted in the SFEs altered by only 0.7–0.8 mJ m^{-2} and the use of the Mg lattice constant is thus shown to be a good approximation.

Nevertheless, it should be noted that our approach based on the YSI does not include more complex thermodynamic aspects of ternary alloys that are related to e.g. ternary phase diagrams where intermetallics and other phases appear and influence, for example, the solubility of solute(s) or thermodynamic stability of ternary alloys. We also note that an alternative solute evaluator was very recently published by Liu *et al* [44] which considers also electronic-structure characteristics of individual solute pairs. This alternative approach can

possibly better capture the thermodynamic complexity of solutes in Mg alloys (see also the recent paper by Cui *et al* [45]). But, in order to do so, it requires quantum-mechanical calculations to be performed for each solute combination and such procedure may not be easily inverted, i.e. identify a solute combination for a given SFE value. In contrast, the YSI was purposely designed to avoid any direct *ab initio* calculations (albeit it is firmly based on our previous quantum mechanical calculations) and its mathematical backbone allows for an inverse materials design. Another specific aspect is interstitial solutes, that typically compare poorly with yttrium using the YSI, and in case of them we suggest the reader to check, for example, the recently published paper by Zhang *et al* [46].

4. Conclusions

We have used quantum-mechanical calculations in order to find relations between the I_1 SFEs in Mg alloys and fundamental atomic properties of elemental solutes. Our analysis showed that the I_1 SFE is (i) strongly anti-correlated to the atomic volume (Pearson correlation coefficient $r = -0.97$), (ii) correlated to the electronegativity ($r = 0.95$) and (iii) logarithmically related to the bulk modulus ($r = 0.90$). Based on these relations, we propose an YSI that combines all three criteria and rationalizes the complexity of prediction of the I_1 SFEs. As this new numerical indicator reproduces the trends of quantum-mechanically computed SFEs for $Mg_{15}X$ with 18 different solutes, we evaluate it for 76 elements from the periodic table of the elements. We have found only one non-RE element, lithium, that we predict to reduce the I_1 SFE. Seeing this limited options in the case of binary Mg alloys, we continue in using the newly introduced YSI parameter in high-throughput theory-guided rapid prototyping of new ternary Mg-alloys with increased ductility.

We extend our YSI analysis to ternary Mg alloys assuming that the physical properties of two solutes can be represented by average values of their individual materials parameters (atomic volume, the electronegativity and the bulk modulus). Out of 2850 solute combinations computed, 133 solute pairs (not including any RE elements) possess a YSI value larger than 0.85 and 11 of them have YSIs higher than 0.95. Subsequent quantum-mechanical calculations of these 11 solute combinations resulted in lower I_1 SFEs (compared with elemental Mg) in case of all of them. Our proposed YSI parameter thus proved to be 100% effective in identifying promising solute candidates. Importantly, the newly introduced numerical quantifier allows the identification of the most promising solutes in a very fast manner and without computationally expensive and lengthy *ab initio* calculations.

Acknowledgments

The authors are grateful to the Deutsche Forschungsgemeinschaft (DFG) for financial support through (i) the project Fundamental investigation of the mechanisms of deformation and recrystallization of cold deformable Mg alloys micro-alloyed with RE elements and microstructure optimization for the development of a new class of Mg-alloys, grant no. YI 103 1-2/ZA 278 6-2, and (ii) the Aachen Institute for Advanced Study in Computational Engineering Science (AICES). MF acknowledges financial support from the Academy of Sciences of the Czech Republic through the Fellowship of Jan Evangelista Purkyně and access to the computational resources provided by the MetaCentrum under the program LM2010005 and the CERIT-SC under the program Centre CERIT Scientific Cloud, part of the Operational Program Research and Development for Innovations, Reg. No. CZ.1.05/3.2.00/08.0144.

References

[1] Agnew S and Nie J 2010 *Scr. Mater.* **63** 671–3
[2] Couling S L 1959 *Acta Metall.* **7** 133–4
[3] Stanford N, Atwell D and Barnett M R 2010 *Acta Mater.* **58** 6773–83
[4] Bohlen J, Yi S, Letzig D and Kainer K U 2010 *Mater. Sci. Eng.* A **527** 7092–8
[5] Sandlöbes S, Zaefferer S, Schestakow I , Yi S and Gonzalez-Martinez R 2011 *Acta Mater.* **59** 429–39
[6] Agnew S, Capolungo L and Calhoun C 2015 *Acta Mater.* **82** 255–65
[7] Sandlöbes S, Friák M, Dick A, Zaefferer S, Yi S, Letzig D, Pei Z, Zhu L-F, Neugebauer J and Raabe D 2012 *Acta Mater.* **60** 3011
[8] Sandlöbes S, Pei Z, Friák M, Zhu L-F, Wang F, Zaefferer S, Raabe D and Neugebauer J 2014 *Acta Mater.* **70** 92–104
[9] Yasi J A, Nogaret T, Trinkle D R, Qi Y, Jr L G H and Curtin W A 2009 *Modelling Simul. Mater. Sci. Eng.* **17** 055012
[10] Yasi J A, Jr L G H and Trinkle D R 2010 *Acta Mater.* **58** 5704–13
[11] Yasi J A, Jr L G H and Trinkle D R 2012 *Acta Mater.* **60** 2350–8
[12] Shin I and Carter E 2012 *Modelling Simul. Mater. Sci. Eng.* **20** 015006
[13] Shin I and Carter E A 2014 *Int. J. Plast.* **60** 58–70
[14] Steinmetz D, Jäpel T, Wietbrock B, Eisenlohr P, Gutierrez-Urrutia I, Saeed-Akbari A, Hickel T, Roters F and Raabe D 2013 Revealing the strain-hardening behavior of twinning-induced plasticity steels: theory, simulations, experiments *Acta Mater.* **61** 494
[15] Cui X-Y, Yen H-W, Zhu S-Q, Zheng R and Ringer S P 2015 *J. Alloys Compd.* **620** 38–41

[16] Kim K-H, Jeon J B and Lee B-J 2015 *Calphad* **48** 27–34
[17] Zhang J, Dou Y, Liu G and Guo Z 2013 *Comput. Mater. Sci.* **79** 564–9
[18] Shang S, Wang W, Zhou B, Wang Y, Darling K, Kecskes L, Mathaudhu S and Liu Z 2014 *Acta Mater.* **67** 168–80
[19] Wang C, Zhang H-Y, Wang H-Y, Liu G-J and Jiang Q-C 2013 *Scr. Mater.* **69** 445–8
[20] Pei Z *et al* 2013 *New J. Phys.* **15** 043020
[21] Hohenberg P and Kohn W 1964 *Phys. Rev.* **136** B864
[22] Kohn W and Sham L J 1965 *Phys. Rev.* **140** A1133
[23] Blöchl P E 1994 *Phys. Rev.* B **50** 17953
[24] Perdew J P, Burke K and Ernzerhof M 1996 *Phys. Rev. Lett.* **77** 3865
[25] Kresse G and Furthmüller J 1996 *Phys. Rev.* B **54** 11169–86
[26] Kresse G and Joubert D 1999 *Phys. Rev.* B **59** 1758–75
[27] Elliott R J 1961 *Phys. Rev.* **124** 346–53
[28] Fisher M E and Selke W 1980 *Phys. Rev. Lett.* **44** 1502–5
[29] Dick A, Hickel T and Neugebauer J 2009 *Steel Res. Int.* **80** 603–8
[30] Hu Q-M and Yang R 2013 *Acta Mater.* **61** 1136–45
[31] Schwarz K, Blaha P and Madsen G 2002 *Comput. Phys. Commun.* **147** 71–76
[32] periodictable.com
[33] Zhu L-F *et al* 2012 *Acta Mater.* **60** 1594
[34] Maisel S, Höfler M and Müller S 2012 *Nature* **491** 740
[35] Hemzalová P, Friák M, Šob M, Ma D, Udyansky A, Raabe D and Neugebauer J 2013 *Phys. Rev.* B **88** 174103
[36] wikipedia.org
[37] Li Z, Gu X, Lou S and Zheng Y 2008 *Biomaterials* **29** 1329–44
[38] Salahshoor M and Guo Y 2012 *Materials* **5** 135–55
[39] Qian M, StJohn D and Frost M 2002 *Scr. Mater.* **46** 649–54
[40] Hauser F, Landon P and Dorn J 1956 *Trans. ASM* **48** 986
[41] Raynor G 1959 *The Physical Metallurgy of Magnesium and Its Alloys* (New York: Pergamon)
[42] Saito N, Mabuchi M, Nakanishi M, Kubota K and Higashi K 1997 *Scr. Mater.* **36** 551–5
[43] Agnew S, Horton J and Yoo M 2002 *Metall. Mater. Trans.* A **33** 851–8
[44] Liu G, Zhang J and Dou Y 2015 *Comput. Mater. Sci.* **103** 97
[45] Cui X-Y, Yen H-W, Zhu S-Q, Zheng R and Ringer S 2015 *J. Alloys Compd.* **620** 38
[46] Zhang J, Liu G and Wei X 2015 *Mater. Lett.* **150** 111